PNAS RESEARCH ARTICLE | EVOLUTION CHEMISTRY OPEN ACCESS

Chemical factors induce aggregative multicellularity in a close unicellular relative of animals

Núria Ros-Rocher[a,b,1], Ria Q. Kidner[c], Catherine Gerdt[c], W. Sean Davidson[d], Iñaki Ruiz-Trillo[a,e], and Joseph P. Gerdt[c,1]

Edited by Joan Strassmann, Washington University in St. Louis, St. Louis, MO; received November 30, 2022; accepted February 14, 2023

Regulated cellular aggregation is an essential process for development and healing in many animal tissues. In some animals and a few distantly related unicellular species, cellular aggregation is regulated by diffusible chemical cues. However, it is unclear whether regulated cellular aggregation was part of the life cycles of the first multicellular animals and/or their unicellular ancestors. To fill this gap, we investigated the triggers of cellular aggregation in one of animals' closest unicellular living relatives—the filasterean *Capsaspora owczarzaki*. We discovered that *Capsaspora* aggregation is induced by chemical cues, as observed in some of the earliest branching animals and other unicellular species. Specifically, we found that calcium ions and lipids present in lipoproteins function together to induce aggregation of viable *Capsaspora* cells. We also found that this multicellular stage is reversible as depletion of the cues triggers disaggregation, which can be overcome upon reinduction. Our finding demonstrates that chemically regulated aggregation is important across diverse members of the holozoan clade. Therefore, this phenotype was plausibly integral to the life cycles of the unicellular ancestors of animals.

multicellularity | aggregation | chemical signaling | *Capsaspora* | lipoproteins

Significance

Whether the first multicellular animals utilized chemical cues to regulate cellular aggregation remains poorly studied. We discovered that aggregation of a unicellular close animal relative is induced by chemical cues, as observed in some animals and other unicellular species. This discovery expands the prevalence of chemically regulated multicellularity in unicellular animal relatives, which suggests that this trait may have been common in the close unicellular ancestors of animals. Our findings also yield a biochemical tool to further dissect the stages of aggregation in an emerging unicellular model and determine the extent of their homology to aggregation mechanisms in animals.

Cellular aggregation arises through the clustering and adhesion of individual cells. This multicellular behavior is broadly distributed across the eukaryotic tree of life, being particularly common in various unicellular organisms (Fig. 1*A*) (1–5). Many of these species, like the amoebozoan *Dictyostelium discoideum*, utilize chemical cues to regulate aggregation in response to harsh environmental conditions (3, 6–16).

Diverse taxa of animals (Opisthokonta, Holozoa) (Fig. 1*A*) also exhibit cellular aggregation during fundamental processes to develop and maintain healthy multicellular tissues. From sponges and cnidarians to vertebrates, animal cells disaggregate and reaggregate for spatial organization of tissues during the early stages of embryonic development (23–25), during inflammatory processes (26, 27), and for tissue regeneration (28–35). A few animal species have been conclusively demonstrated to use soluble chemical cues to regulate their aggregation phenotypes (6, 27, 29, 32, 36–42). However, it is unclear how chemically regulated cellular aggregation evolved in the animal lineage and whether it was part of the life cycles of the latest unicellular ancestors of animals.

Recently, extant unicellular relatives of animals (i.e., unicellular holozoans, Fig. 1*A*) have become powerful models to reconstruct which genes and biological traits were likely present in the unicellular ancestors of animals (43, 44). For instance, comparative genomic studies between animals and unicellular holozoans revealed that the genomes of many unicellular holozoans encode genes homologous to those that are essential for animal development and multicellularity. These include components of the animal cell adhesion machinery, developmental transcription factors, and cell–cell communication proteins, which are thus inferred to be present in their common unicellular ancestors (43, 45). Similarly, analyses of their lifestyles showed that unicellular holozoans exhibit a diversity of multicellular phenotypes, including multicellular colonies formed through cellular aggregation (21, 46). These findings suggest that the life cycles of the unicellular ancestors most likely integrated single-celled states and transient multicellular phenotypes. However, it remains obscure how unicellular ancestors regulated most multicellular phenotypes and, particularly, whether they could have employed similar mechanisms to those observed in animals.

Among unicellular holozoans, the filasterean amoeba *Capsaspora owczarzaki,* hereafter *Capsaspora,* can form multicellular aggregates (21, 47, 48) that are morphologically similar to aggregates formed by animal cells, particularly sponges and hydra during whole-body regeneration (Fig. 1 *B* and *C*) (21, 28, 32, 33). These animal-like *Capsaspora* aggregates exhibit elevated expression of many genes homologous to those involved in cell adhesion in animals (21, 47, 48). Nevertheless, little is known about how *Capsaspora* regulates its aggregative phenotype.

Author affiliations: [a]Department of Functional Genomics and Evolution, Institut de Biologia Evolutiva (Consejo Superior de Investigaciones Científicas-Universitat Pompeu Fabra), 08003 Barcelona, Spain; [b]Department of Cell Biology and Infection and Department of Developmental and Stem Cell Biology, Institut Pasteur, 75015 Paris, France; [c]Department of Chemistry, Indiana University, Bloomington, IN 47405; [d]Department of Pathology and Laboratory Medicine, University of Cincinnati, Cincinnati, OH 45221; and [e]Institució Catalana de Recerca i Estudis Avançats, 08010 Barcelona, Spain

Author contributions: N.R.-R. and J.P.G. designed research; N.R.-R., R.Q.K., C.G., and J.P.G. performed research; N.R.-R., R.Q.K., C.G., W.S.D., and J.P.G. contributed new reagents/analytic tools; N.R.-R., R.Q.K., and J.P.G. analyzed data; I.R.-T. and J.P.G. acquired funding; and N.R.-R., I.R.-T., and J.P.G. wrote the paper.

The authors declare no competing interest.

This article is a PNAS Direct Submission.

Copyright © 2023 the Author(s). Published by PNAS. This open access article is distributed under Creative Commons Attribution-NonCommercial-NoDerivatives License 4.0 (CC BY-NC-ND).

[1]To whom correspondence may be addressed. Email: nuria.ros@pasteur.fr or jpgerdt@iu.edu.

This article contains supporting information online at https://www.pnas.org/lookup/suppl/doi:10.1073/pnas.2216668120/-/DCSupplemental.

Published April 24, 2023.

Downloaded from https://www.pnas.org by 84.18.99.124 on August 3, 2023 from IP address 84.18.99.124.

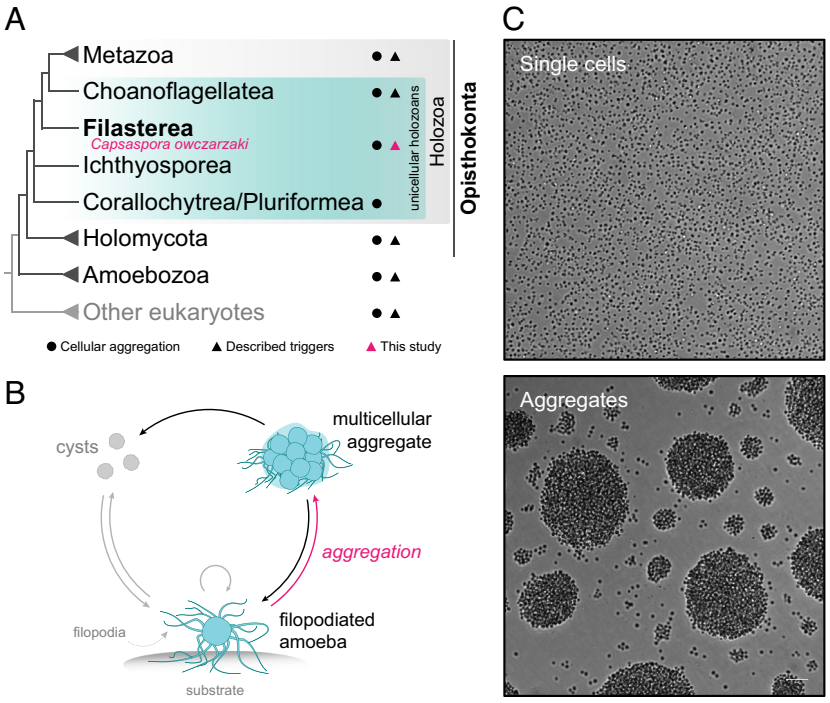

Fig. 1. *Capsaspora* transitions from a unicellular to a multicellular life stage. (*A*) Animals (Metazoa) and their closest unicellular relatives, including *Capsaspora* (Filasterea), form the Holozoa clade within the Opisthokonta supergroup. The phylogenetic relationships of selected taxa are based on several recent phylogenomic studies (17–20). Uncertain positions are represented with polytomies. (*B*) Life stages of *Capsaspora* under culture conditions. The trophic proliferative cells are filopodiated amoebae adhered to the substrate (adherent stage). These amoebae can detach from the substrate and form multicellular aggregates (aggregative stage). In response to crowding or stress, cells from both the adherent and the aggregative stages can encyst by retracting the filopodia (cystic stage). Arrows indicate directionality of each transition, with an emphasis on aggregation (pink arrow) and disaggregation (black arrows). Loop arrow indicates cell division in adherent cells (21, 22). (*C*) *Capsaspora* single cells at the adherent stage (*Top*) transition to multicellular aggregates (*Bottom*). (Scale bar, 100 μm.)

Therefore, we sought to characterize how *Capsaspora* regulates cellular aggregation and compare it to aggregation regulation in present-day animals and other aggregating unicellular species. Because some animal cells and unicellular species form aggregates in response to chemical cues (7, 8, 28, 29, 49–52), we specifically asked if *Capsaspora* also employs extracellular chemical signals to regulate its aggregative behavior. We discovered that *Capsaspora* aggregation, like cellular aggregation in some animals, choanoflagellates, and some other unicellular species, indeed depends on chemical cues. We identified the chemical cues to be calcium ions and lipids present in lipoproteins. We also discovered that *Capsaspora* aggregation is a reversible process that depends on the concentration of the cues. Moreover, the cues only induce aggregation of viable *Capsaspora* cells, suggesting that an active cellular response regulates aggregation. Further molecular studies are needed to determine the degree to which this regulated aggregation behavior is genetically conserved with animals. Nonetheless, this finding adds to the increasing prevalence of chemically regulated multicellularity in unicellular animal relatives, which suggests that the close unicellular ancestors of animals may have been capable of chemically regulated multicellular phenotypes.

Results

Fetal Bovine Serum (FBS) Contains Chemical Factor(s) Necessary for Aggregation in *Capsaspora*. *Capsaspora* aggregates have previously been induced using physical forces by gentle orbital agitation of amoeboid cells in a manner similar to sponge primmorph induction (21, 28, 47, 48). Since some animals and other unicellular species secrete chemical cues to promote cell aggregation (7, 37, 51, 53), we initially inquired whether *Capsaspora* aggregates could be induced by secreted cues from aggregating cultures under agitation conditions. However, we were unable to observe that behavior.

We then asked whether environmental chemical factors could induce aggregation in *Capsaspora*. During the aggregation process, *Capsaspora* cells are maintained in growth media: a nutrient-rich buffered solution containing 1% (w/v) peptone, 1% (w/v) yeast extract, and 10% (v/v) heat-inactivated FBS. To determine if any of these components were necessary for aggregation, we agitated *Capsaspora* cultures in variations of the media lacking each of these components. We first modified the previously reported aggregation assay (21) to test multiple conditions and reduce the amount of sample used (*SI Appendix*, Fig. S1*A*) and also incorporated an automated image analysis pipeline to distinguish between aggregates and single cells based on particle size (*SI Appendix*, Fig. S2). Using this setup, we found that cells agitated in FBS-free media were unable to form aggregates, suggesting that chemical cues from FBS are required to induce aggregation in *Capsaspora* (Fig. 2 *A* and *B*).

Chemical Induction Is Sufficient for Aggregation Even in the Absence of Physical Agitation. In the process of assessing the aggregation effect of FBS, we serendipitously observed that *Capsaspora* cells can aggregate without physical agitation. In fact, cells in FBS-free media formed small aggregates within 20 min after addition of 10% (v/v) FBS *in the absence of orbital agitation* (Fig. 2*C*, *SI Appendix*, Fig. S1*C*, and Movie S1). This aggregation effect was even more pronounced upon addition of 30% (v/v) FBS, which induced larger aggregates within the next 10 min after induction, suggesting that physical agitation forces are not necessary to induce aggregation (Fig. 2*C*, *SI Appendix*, Fig. S1*C*,

Downloaded from https://www.pnas.org by 84.18.99.124 on August 3, 2023 from IP address 84.18.99.124.

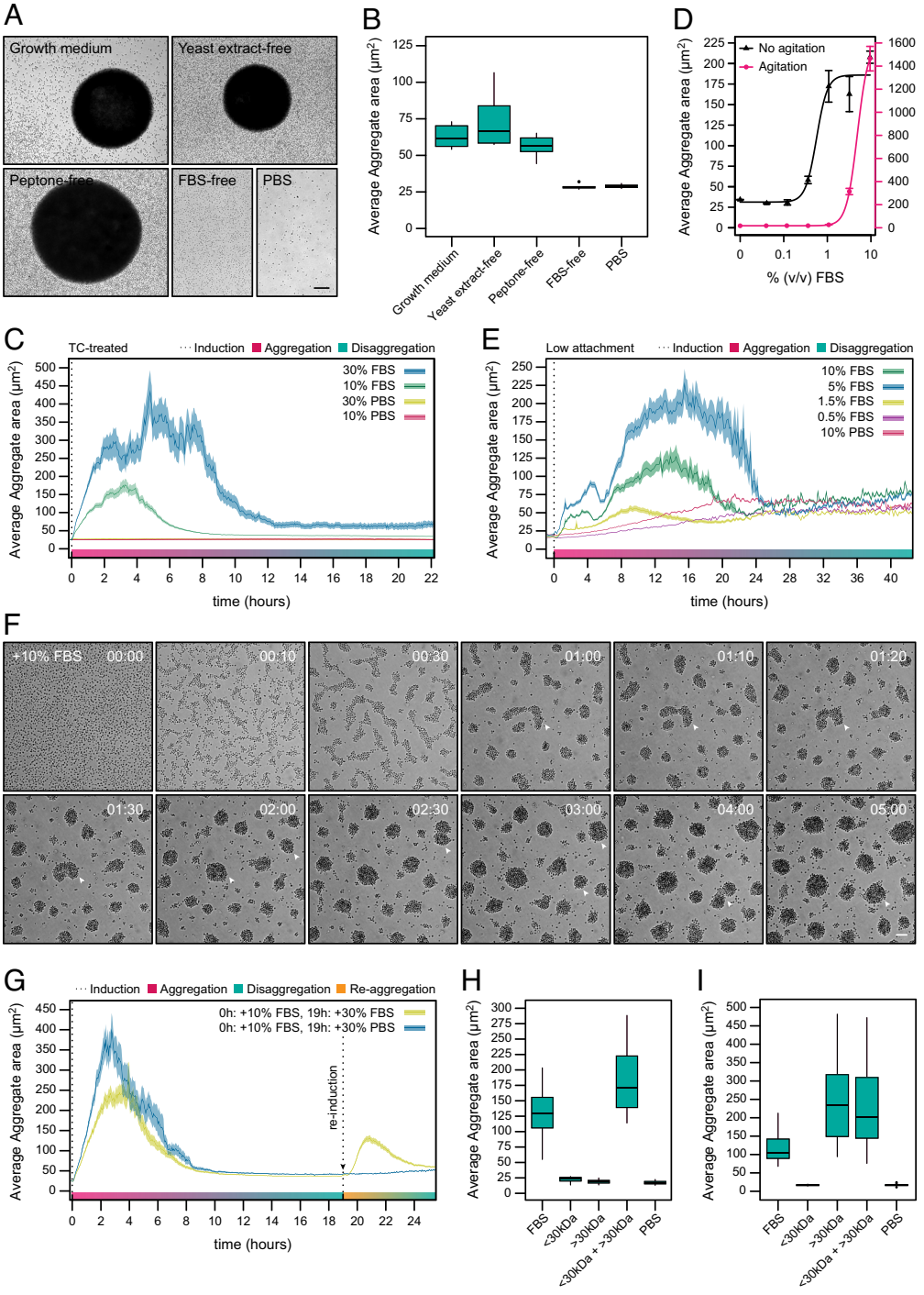

Fig. 2. Chemical cues from FBS are necessary to induce aggregation in *Capsaspora*. (*A*) Microscopy images of *Capsaspora* aggregates induced under agitation conditions in growth medium and medium lacking some of its major components. Aggregates failed to form in FBS-free media and in 1× phosphate buffered saline (PBS) (negative control) (*SI Appendix*, Fig. S1*A* assay). (Scale bar, 100 μm.) (*B*) Data from each test condition in *A* are represented as boxplots, showing the median aggregate area (thick black bar) and interquartile ranges from three independent biological replicates. Figure related to *SI Appendix*, Fig. S2. (*C*) FBS is sufficient to induce aggregation in the absence of physical agitation. Aggregation dynamics over time induced by 10% and 30% (v/v) FBS in the absence of physical agitation using tissue culture–treated (TC-treated) 12-well plates (*SI Appendix*, Fig. S1*C* assay). A 10% (v/v) and 30% (v/v) of 1× PBS were used as negative controls. Data are represented as the average aggregate area (thick line) ± SEM (shadow) from three biological replicates. Quantification plot related to Movies S1 and S2. (*D*) Aggregation of *Capsaspora* cells induced by dose responses of FBS in agitation (*SI Appendix*, Fig. S1*B* assay) and in the absence of agitation conditions (*SI Appendix*, Fig. S1*D* assay). Data are represented as the average aggregate area ± SEM from three independent biological replicates. (*E*) Aggregation dynamics over time induced by serial dilutions of FBS (v/v) in the absence of agitation conditions in ultralow attachment 96-well plates (*SI Appendix*, Fig. S1*D* assay). A 10% (v/v) of 1× PBS was used as a negative control. Data are represented as the average aggregate area (thick line) ± SEM (shadow) from three independent biological replicates in no agitation conditions. Quantification plot related to Movies S3 and S4. (*F*) Aggregate formation induced by 10% (v/v) of FBS (time 0) in ultralow attachment plates related to Movie S3 (*SI Appendix*, Fig. S1*D* assay and *SI Appendix*, Fig. S3). White arrowheads track early aggregate formation and aggregate fusion events (agglomeration). Time represents hh:mm. (Scale bar, 100 μm.) (*G*) Aggregation and reaggregation dynamics over time in the absence of physical agitation using 12-well plates (*SI Appendix*, Fig. S1*C* assay). Aggregates were induced with a 10% (v/v) of FBS (time 0) and monitored until disaggregation into single cells. After ~19 h, either a 30% (v/v) of FBS was added to induce reaggregation (yellow curve), or a 30% (v/v) of 1× PBS was added as a negative control (blue curve). Data are represented as the average aggregate area (thick line) ± SEM (shadow) from three biological replicates. Quantification plot related to Movie S5. A similar result was observed for reaggregation induced with 10% (v/v) of FBS (*SI Appendix*, Fig. S4). (*H*) The combination of <30-kDa and >30-kDa FBS fractions induce aggregation of *Capsaspora* cells. Cells were induced with 10% (v/v) of whole FBS, 10% (v/v) of <30-kDa FBS fraction, 10% (v/v) of >30-kDa FBS fraction, or a combination of both fractions (5% (v/v) each) in agitation conditions (*SI Appendix*, Fig. S1*B* assay). A 10% (v/v) of 1× PBS was used as a negative control. Data are represented as boxplots, showing the median aggregate area (thick black bar) and interquartile ranges from three independent biological replicates. (*I*) The >30-kDa FBS fraction is sufficient to induce reaggregation of *Capsaspora* cells. Aggregation was induced with 10% (v/v) of FBS and monitored until disaggregation (~72 h). At this point, disaggregated cells were reinduced with either 10% (v/v) of FBS, 10% (v/v) of <30-kDa FBS fraction, 10% (v/v) of >30-kDa FBS fraction, or a combination of both fractions (5% (v/v) each) in agitation conditions (*SI Appendix*, Fig. S1*B* assay). A 10% (v/v) of 1× PBS was used as a negative control. Data are represented as boxplots, showing the median aggregate area (thick black bar) and interquartile ranges from three independent biological replicates.

and Movie S2). In fact, *Capsaspora* aggregates are often randomly observed in very dense stationary cultures (21). Agitation may encourage *Capsaspora* aggregation by preventing amoeboid cells from attaching to tissue culture–treated surfaces, therefore leading to greater opportunities for cell–cell contact, adhesion, and ultimately aggregation, as observed in sponges (54, 55). To test this hypothesis, we analyzed the effect of FBS in a dose–response experiment using "ultralow attachment" surfaces in the absence of agitation (Fig. 2*D*, *SI Appendix*, Figs. S1*D* and S3, and Movies S3 and S4). Indeed, we found that *Capsaspora* cells aggregate at even 1% (v/v) FBS in the absence of agitation compared to ~3% (v/v) FBS in agitation conditions, lending support to the hypothesis that aggregation is primarily regulated by the presence of chemical cue(s) in FBS (Fig. 2 *D*–*F*, *SI Appendix*, Fig. S1 *B* and *D*,

Downloaded from https://www.pnas.org by 84.18.99.124 on August 3, 2023 from IP address 84.18.99.124.

and Movie S4). In the low attachment plates, cells aggregated 10 min after induction (Fig. 2 *E–F*, *SI Appendix*, Fig. S3, and Movies S3 and S4). Upon induction, single cells aggregated into small round aggregates (Fig. 2 *E–F*, *SI Appendix*, Fig. S3, and Movies S3 and S4). In the next few hours, small aggregates began fusing together into larger aggregates (agglomeration), a process that lasted ~24 h (Fig. 2 *E–F*, *SI Appendix*, Fig. S3, and Movie S3). After ~26 h, all aggregates disassembled into single cells again (disaggregation) (Fig. 2*E*, *SI Appendix*, Fig. S3, and Movies S3 and S4). Altogether, these data confirmed that agitation is not necessary to induce aggregation but rather helps make the cells more sensitive to the chemical inducer(s) in FBS, which are sufficient to induce aggregation in *Capsaspora*.

Chemical Induction of Aggregation Is Reversible. After finding that chemical factor(s) in FBS are necessary to induce aggregation in *Capsaspora*, we asked whether FBS can induce reaggregation of single cells coming from disassembled aggregates. In fact, reaggregation of independent cells after tissue dissociation is a common phenomenon frequently observed in sponge cells, hydra cells, and other animal cell lines which, in some cases, is also promoted by serum components (40, 54, 55). To this end, we first monitored the aggregation–disaggregation process of *Capsaspora* cells induced with 10% (v/v) FBS (Fig. 2*G*, *SI Appendix*, Figs. S1 *B* and *C* and S4, and Movie S5). Then, once the aggregates were completely disaggregated into single cells, we examined the effect of readdition of 10% or 30% (v/v) of FBS. Indeed, we found that chemical induction rapidly stimulated reaggregation of cells within 10 min, confirming that *Capsaspora* aggregation is reversible (Fig. 2*G*, *SI Appendix*, Fig. S4, and Movie S5).

Two Soluble FBS Components (One Small and One Large) Are Required for Aggregation. To identify the serum component(s) that induce *Capsaspora* aggregation and reaggregation, we performed an activity-guided fractionation of FBS. We first used a 30-kDa MW cutoff spin filter to separate FBS into small (<30-kDa) and large (>30-kDa) serum components. These two fractions were then tested for their ability to induce aggregation using the aggregation assay with orbital agitation (Fig. 2*H* and *SI Appendix*, Fig. S1*B*). Surprisingly, neither serum fraction was sufficient to induce aggregation alone. However, when both fractions were recombined, the combination induced *Capsaspora* aggregation. These results indicated that at least two soluble serum components are required for aggregation, one that is <30-kDa and one that is >30-kDa (Fig. 2*H*).

In parallel, we also assessed the reaggregation activity of both FBS fractions after disaggregation (Fig. 2*I* and *SI Appendix*, Fig. S1*B*). Interestingly, we found that the >30-kDa FBS fraction alone was sufficient to induce reaggregation. This result suggested that the large FBS fraction component(s) were depleted over time, leading to disaggregation (Fig. 2*I* and *SI Appendix*, Fig. S1*B*). Then, readdition of the >30-kDa component(s) triggered reaggregation. In contrast, the <30-kDa component(s) likely persisted through the aggregation–disaggregation cycle.

The Small Active Serum Component Is Calcium Ions. We then sought to determine the chemical nature of the small active serum component(s). We further used a 3-kDa MW cutoff filter to isolate even smaller serum components, and we found that this <3-kDa FBS fraction induced *Capsaspora* aggregation in the presence of the >30-kDa FBS material (not shown). Next, we performed solvent extractions from freeze-dried <3-kDa FBS material. The solvents included a series of chloroform, methanol, and finally water in order to separate organic-soluble components (such as lipids and polar metabolites) and water-soluble and water-insoluble salts. After testing the aggregation activity of each of the recovered extracts in combination with the >30-kDa FBS material, we found that the only active fraction was the one containing salts that did not redissolve in any solvent (chloroform, methanol, or water) (*SI Appendix*, Fig. S5).

We then asked which factor(s) in the insoluble fraction could be active. Calcium ions are prevalent in FBS (~3 mM) (56), and they have the potential to form insoluble salts. Indeed, our FBS contained 3.7 ± 0.2 mM Ca^{2+}. We thus hypothesized that calcium ions could be the necessary component for aggregation because of their roles in promoting cadherin-mediated cell–cell adhesion in many organisms (57) and promoting cellular aggregation in sponges, yeasts, and other unicellular species (38, 52, 58). We therefore tested the ability of $CaCl_2$ to induce *Capsaspora* aggregation in the presence of the >30-kDa FBS fraction in a dose–response experiment. Indeed, Ca^{2+} was able to induce *Capsaspora* aggregation at concentrations lower than 0.1 mM (Fig. 3*A*). Therefore, Ca^{2+} is sufficient to induce aggregation when combined with >30-kDa FBS components.

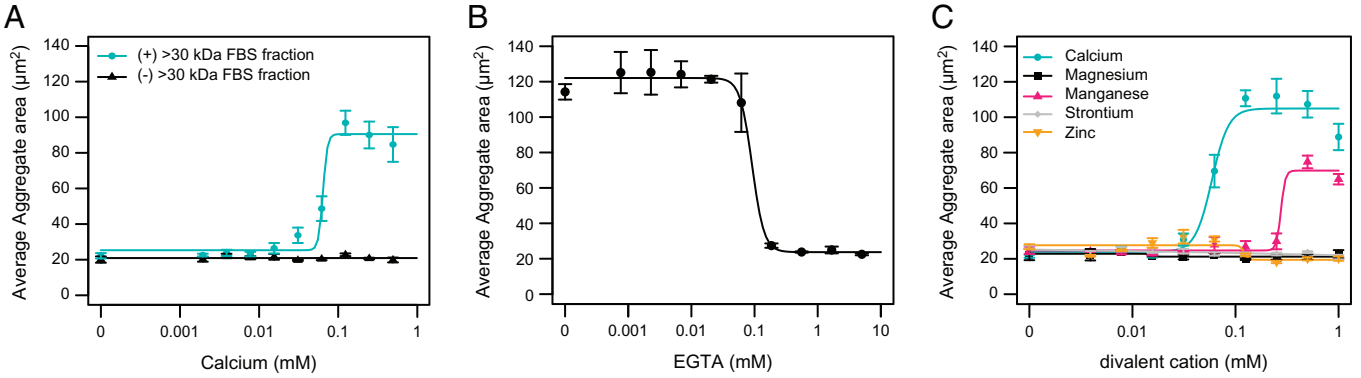

Fig. 3. The small (<30-kDa) serum active component is calcium ions. (*A*) Calcium ions in combination with 5% (v/v) >30-kDa FBS fraction induce aggregation in *Capsaspora*. (*B*) Treatment with calcium-chelating agent ethylene glycol-bis(β-aminoethyl ether)-N,N,N′,N′-tetraacetic acid (EGTA) impairs aggregation of *Capsaspora* cells induced with 5% (v/v) FBS. (*C*) *Capsaspora* cells induced with 5% (v/v) >30-kDa FBS fraction and chloride salts of various divalent cations aggregate only in the presence of calcium chloride at physiological concentration ranges. Manganese chloride induces weaker aggregation in the presence of 5% (v/v) >30-kDa FBS fraction at high concentrations (0.3 mM). Results in *A–C* are shown as the average aggregate area of three independent experiments ± SEM. All experiments are performed following *SI Appendix*, Fig. S1*D* assay. Figure related to *SI Appendix*, Fig. S5.

Downloaded from https://www.pnas.org by 84.18.99.124 on August 3, 2023 from IP address 84.18.99.124.

To test if Ca^{2+} is strictly necessary for aggregation in *Capsaspora*, we depleted available Ca^{2+} with ethylene glycol-bis(β-aminoethyl ether)-N,N,N′,N′-tetraacetic acid (EGTA)—a chelating agent with especially high affinity for calcium ions. We performed an EGTA dose–response experiment with *Capsaspora* cells induced with FBS and found that EGTA impaired aggregation at concentrations as low as ~0.1 mM (Fig. 3*B*). To rule out the involvement of other divalent metal cations, we tested the activity of the chloride salts of magnesium, manganese, strontium, and zinc. None of these cations were capable of inducing aggregation at physiological concentrations (Fig. 3*C*). We observed weak aggregation induced by $MnCl_2$ but only at concentrations of 0.3 mM and above, which is far higher than 10% (v/v) FBS would afford (~0.1 μM, see refs. 56 and 59) (Fig. 3*C*). Altogether, these findings confirmed that calcium ions are necessary and sufficient to trigger aggregation of *Capsaspora* cells in the presence of >30-kDa FBS components.

The Combination of Low-Density Lipoproteins (LDLs) and Calcium Ions Is Sufficient to Induce Aggregation. Next, we sought to uncover the chemical nature of the large active serum component(s). The aggregation activity of the >30-kDa FBS fraction was sensitive to protease treatment, suggesting that the large active serum component(s) is proteinaceous (Fig. 4*A*). We therefore separated all proteins from the >30-kDa FBS material by ammonium sulfate precipitation and tested the aggregation activity of the recovered precipitates in combination with 0.2 mM $CaCl_2$ (*SI Appendix*, Fig. S6). The resulting active fractions from the ammonium sulfate precipitation (*SI Appendix*, Fig. S6 *D and E*) *D* and *E* were next separated by anion exchange chromatography and tested for their aggregation activity again (*SI Appendix*, Fig. S7). The active anion exchange fractions (*SI Appendix*, Fig. S7*B*) were in turn further separated by size exclusion chromatography (*SI Appendix*, Fig. S8). The active size exclusion fractions that exhibited robust aggregation (*SI Appendix*, Fig. S8*C*) were later separated by sodium dodecyl sulfate–polyacrylamide gel electrophoresis (SDS-PAGE) and analyzed by Coomassie staining (*SI Appendix*, Fig. S9 *A* and *B*). We finally determined the protein content of all visible unique bands from the active fractions via mass spectrometry. The major protein in all seven purified bands matched a single ~515-kDa protein—Apolipoprotein B100 (ApoB100) (*SI Appendix*, Fig. S9 *A* and *B* and Dataset S1).

ApoB100 is the primary organizing protein of LDLs and very low–density lipoproteins, two major transporters of poorly soluble lipids, including cholesterol, cholesteryl esters, and triglycerides (60, 61). We therefore hypothesized that either ApoB100, itself, induces aggregation or whole lipoprotein particles induce aggregation. Pure ApoB100 (plus 0.3 mM $CaCl_2$) failed to induce

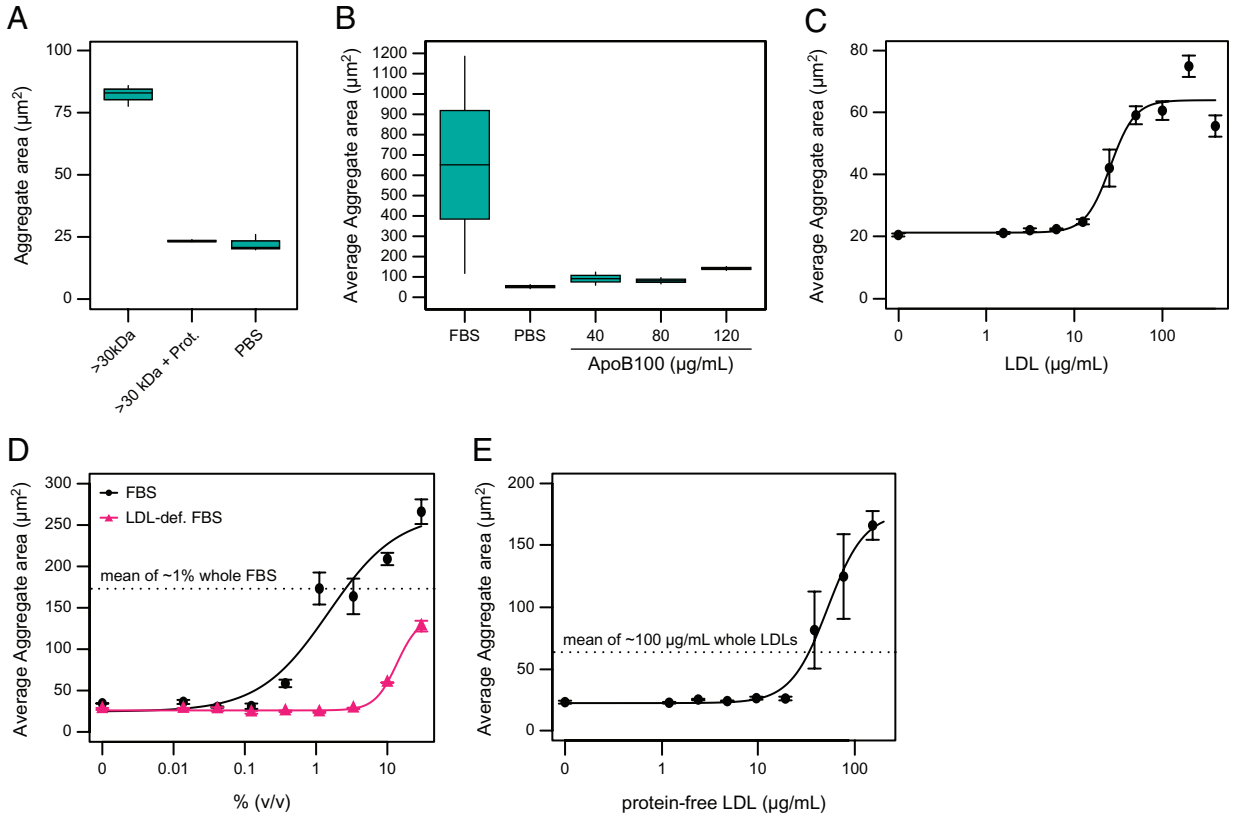

Fig. 4. The combination of LDLs and calcium ions induces aggregation in *Capsaspora*. (*A*) 5% (v/v) of proteinase-treated >30-kDa FBS fraction shows reduced aggregation activity compared to 5% (v/v) of untreated >30-kDa fraction in combination with 0.2 mM $CaCl_2$. A 10% (v/v) treatment of 1× PBS was used as a negative control. Data are represented as boxplots, showing the median aggregate area (thick black bar) and interquartile ranges from three independent biological replicates. Figure related to *SI Appendix*, Figs. S6–S8. (*B*) ApoB100 in combination with 0.3 mM $CaCl_2$ does not fully recapitulate the aggregation activity of 10% (v/v) FBS. Data are represented as boxplots, showing the median aggregate area (thick black bar) and interquartile ranges from two independent biological replicates in agitation conditions (*SI Appendix*, Fig. S1*B* assay). A 10% (v/v) of FBS was used as a positive control, and a 10% (v/v) of 1× PBS was used as a negative control. Figure related to *SI Appendix*, Fig. S9 and Dataset S1. (*C*) Dose response of whole LDLs (plus 0.2 mM $CaCl_2$) in the absence of agitation conditions (*SI Appendix*, Fig. S1*D* assay). Data are represented as the average aggregate area ± SEM from three independent biological replicates. (*D*) Dose responses of whole FBS and LDL-deficient FBS (both in the presence of 0.2 mM $CaCl_2$) in the absence of agitation (*SI Appendix*, Fig. S1*D* assay). LDL-deficient FBS has reduced activity, inducing weak aggregation at 30% (v/v) concentrations, whereas whole FBS induces aggregation at ~1% (v/v). Data are represented as the average aggregate area ± SEM from three independent biological replicates. Figure related to *SI Appendix*, Fig. S10. (*E*) Dose response of pfLDLs (plus 0.2 mM $CaCl_2$) in the absence of agitation conditions (*SI Appendix*, Fig. S1*D* assay). Data are represented as the average aggregate area ± SEM from three independent biological replicates.

Downloaded from https://www.pnas.org by 84.18.99.124 on August 3, 2023 from IP address 84.18.99.124.

robust aggregation (Fig. 4*B* and *SI Appendix*, Fig. S9*C*). In fact, ApoB100 appeared toxic at high concentrations (*SI Appendix*, Fig. S9*C*), in agreement with previous work using mammalian cells (62). However, whole LDLs (plus 0.2 mM $CaCl_2$) were sufficient to induce aggregation at concentrations as low as ~10 μg/mL, recapitulating the aggregation activity of our 10% (v/v) FBS control (Fig. 4*C*). To further confirm the aggregation activity of LDLs, we obtained serum that was >95% deficient in lipoproteins, including LDLs (*SI Appendix*, Fig. S10 *A–C*). We found that LDL-deficient FBS was a substantially less potent aggregation inducer than whole FBS (Fig. 4*D* and *SI Appendix*, Fig. S10*D*), confirming the importance of LDLs to induce aggregation.

Lipids Are the Active Components of LDLs. Our finding that *Capsaspora* aggregation is induced by whole LDLs left two major questions. First, LDLs are complexes isolated from natural sources, which contain small amounts of impurities. Therefore, the question remained whether the induction response was truly due to LDLs or instead caused by slight impurities that associate with LDLs. Second, the ecological relevance of LDLs for *Capsaspora* aggregation remained cryptic, especially because LDLs are a vertebrate innovation (63) that *Capsaspora* might not encounter in its natural environment. In fact, *Capsaspora* has only been isolated from snails (22, 64), and its common ancestors with animals would have existed in a world without LDLs. Thus, LDLs are unlikely to be a relevant aggregation cue for present-day *Capsaspora* and its premetazoan ancestors. Therefore, the question remained if a more ecologically relevant aggregation inducer exists. To address both of these questions, we sought to determine if pure and ubiquitous components of LDLs could induce aggregation.

Given that the pure ApoB100 protein failed to induce *Capsaspora* aggregates like whole LDLs, we hypothesized that the lipid components of LDLs could be responsible for inducing aggregation (in combination with calcium ions). We generated protein-free LDL particles (pfLDLs) composed of synthetic lipids representing the five major lipid classes in LDLs (50% 1-palmitoyl-2-oleoyl-glycero-3-phosphocholine [POPC], 5% oleoyl sphingomyelin, 13% cholesterol, 4% triolein, and 28% cholesteryl oleate) (65). Transmission electron microscopy (TEM) images and dynamic light scattering measurements confirmed the formation of lipid particles with an average diameter of 105 nm (*SI Appendix*, Fig. S11), and LC-MS/MS analysis confirmed the incorporation of all the lipids at the percentages listed above (*SI Appendix*, Table S1). Indeed, these pfLDLs were sufficient to induce aggregation (in the presence of calcium ions) (Fig. 4*E*). The EC_{50} of induction was 53 μg/mL, which is comparable to the potency of LDLs (EC_{50} ~26 μg/mL). Therefore, the lipids of LDLs appear to be the true aggregation cue. However, given our previous observation that protease digestion inactivated the initial active >30-kDa FBS material, it is likely that the protein component(s) of the LDLs are important for the long-term stability and delivery of the inducing lipid(s) to the cells. It remains to be determined if one lipid is sufficient to induce aggregation or if a mixture is required.

Dynamic Lipoprotein Concentration Regulates the Aggregative State of *Capsaspora*. Given that aggregates dissociated over time (and reformed after addition of the lipoprotein-containing serum fractions), we inquired whether LDLs were depleted over the course of the aggregation experiment. To test this, we analyzed the LDL content during the course of aggregation and disaggregation using an anti-LDL antibody. Our findings revealed that the concentration of LDL did, in fact, significantly decrease in the time leading up to disaggregation (Fig. 5*A* and *SI Appendix*, Fig. S12). These results led us to hypothesize that the LDLs were depleted by *Capsaspora* metabolism. To test this hypothesis, we assessed the localization of LDLs using immunofluorescence microscopy. We observed LDLs localized in intracellular vesicles in *Capsaspora* aggregates and adherent cells immunostained with anti-LDL antibodies (Fig. 5*B* and *SI Appendix*, Fig. S13). Together, these findings indicate that *Capsaspora* engulfs LDLs, thereby depleting them from the media. Therefore, the dynamic concentration of lipoproteins regulates the aggregative state of *Capsaspora*: High concentrations of lipoproteins induce aggregation; however, as lipoproteins are depleted, aggregates disassemble and only reassemble when lipoprotein concentrations are restored.

Only Viable *Capsaspora* Cells Aggregate. Finally, we began to dissect the mechanism by which the active components from FBS induce aggregation in *Capsaspora*. In sponges, cellular aggregation is induced by soluble proteoglycan complexes called sponge *aggregation factors* (AFs) (37, 38, 53, 66). These aggregation inducers function as multivalent adhesives to physically link sponge cells to each other, even when those cells are formalin-fixed (i.e., metabolically inactive) in rotationally induced aggregation experiments (54, 66). In other unicellular species, like *D. discoideum,* yeasts, or algae, the cues induce an active cellular response that results in aggregation (50–52). Actin staining revealed that cells within *Capsaspora* aggregates appear directly linked to each other through filopodia (Fig. 5*B* and *SI Appendix*, Fig. S13). Because we also observed distinct patches of LDLs localized along filopodia within aggregates (Fig. 5*B* and *SI Appendix*, Fig. S13), we inquired whether serum-supplied lipoproteins trigger *Capsaspora* aggregation by an adhesive mechanism like sponge AFs. We thus fixed *Capsaspora* cells with increasing concentrations of formaldehyde and later induced aggregation with 10% (v/v) FBS in orbital agitation (Fig. 5*C* and *SI Appendix*, Fig. S1*B*). Unlike sponge cells, we found that formalinized *Capsaspora* cells were *unable* to aggregate even in the presence of 10% (v/v) FBS. Although we cannot rule out the possibility that formaldehyde treatment directly disrupts an LDL–*Capsaspora* adhesive interaction, this result suggests that LDLs are *not simply a "glue"* that links passive cells together. Instead, LDLs likely induce aggregation through an active biological response from living *Capsaspora* cells in a manner reminiscent to the active cellular responses observed in other unicellular species.

Discussion

We have discovered that chemical cues induce aggregative multicellularity in *Capsaspora*, one of the closest unicellular relatives of animals (Fig. 5*D*). In the presence of these cues, *Capsaspora* amoebae form large spherical aggregates that resemble the initial aggregated stages whereby dissociated animal cells reaggregate and develop into new viable organisms (23, 29–31, 33, 35). Thus, the fact that early-branching animals, the choanoflagellate *S. rosetta* (49) and *Capsaspora* utilize chemical cues to regulate aggregation is suggestive that the unicellular ancestors of animals also employed chemical cues to regulate aggregation.

We found that two chemical factors are necessary for *Capsaspora* aggregation. The first is calcium ions [corroborated by recent work from Phillips et al. (67)]. Calcium ions are similarly required for the aggregation of *D. discoideum,* yeasts, and sponge cells. During *D. discoideum* aggregation, intracellular calcium ion dynamics are linked to cAMP levels, that in turn regulate chemotaxis and stalk cell differentiation (58). Furthermore, calcium ions act as secondary messengers in many signaling pathways (68) and may be required for transduction of the *Capsaspora* aggregation induction signal. Alternatively, calcium

Downloaded from https://www.pnas.org by 84.18.99.124 on August 3, 2023 from IP address 84.18.99.124.

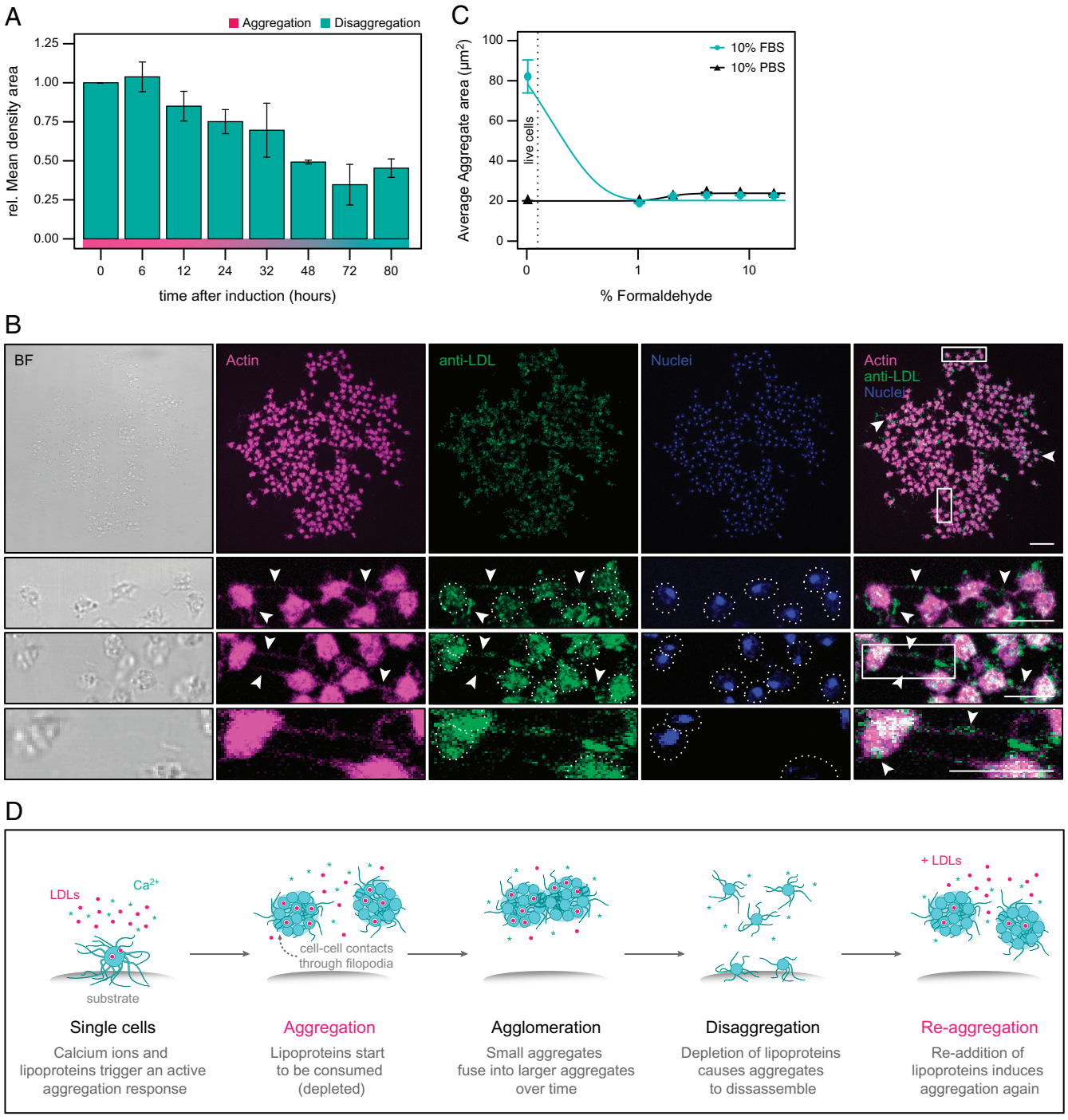

Fig. 5. Dynamic lipoprotein concentration regulates an aggregation response in viable *Capsaspora* cells. (*A*) LDLs are depleted over time during the aggregation–disaggregation process. Quantification of LDL content of media supernatants collected from cells induced with 10% (v/v) FBS (0 h) by western blot show progressive disappearance of LDLs in the time leading up to disaggregation (72 to 80 h). Data are represented as the mean density areas relative to 0 h time point ± SD from two independent biological replicates. Figure related to *SI Appendix*, Figs. S4 *A* and *B* and S12. (*B*) LDLs are localized in intracellular small foci and in patches along filopodia in a *Capsaspora* aggregate induced with 10% (v/v) of FBS. Shown is a maximum z projection of an aggregate (*Upper*) stained with phalloidin (magenta) to mark filamentous actin (cell body and filopodia), an anti-LDL antibody to mark LDLs (green), and DRAQ5 to mark nuclei (blue). A merge of phalloidin and anti-LDL staining shows that LDLs localize in the interior of cells and filopodia (white arrows). A representative bright-field (BF) stack image is shown. *Lower* panels represent two zoom-in maximum z-projection images (white squares) of the aggregate stained as before. (Scale bar in the *Upper* panel represents 25 µm and 10 µm in all magnified *Lower* panels.) Figure related to *SI Appendix*, Fig. S13. (*C*) *Capsaspora* cells fixed with increasing concentrations of formaldehyde do not aggregate upon induction with 10% (v/v) of FBS. Data are represented as the average aggregate area ± SEM from three independent biological replicates (*SI Appendix*, Fig. S1*B* assay). A 10% (v/v) of 1× PBS was used as a negative control. (*D*) *Capsaspora* cells aggregate in the presence of calcium ions and lipoproteins, which trigger an active aggregation response. During the course of aggregation, smaller aggregates fuse together into larger aggregates (agglomeration) while consuming lipoproteins. Depletion of lipoproteins leads aggregates to disassemble into single cells again (disaggregation). Readdition of lipoproteins induces reaggregation of *Capsaspora* cells.

ions are essential for stabilizing many cell–cell adhesion molecules. For example, calcium ions stabilize the lectins responsible for yeast asexual flocculation (52). In sponges, calcium ions likely play a structural role stabilizing cell–cell contacts through associations of cell surface sponge AFs (37, 38, 53, 66). Calcium ions also stabilize other animal cell adhesion molecules, such as cadherins and integrins (69, 70). Indeed, some genes predicted to encode calcium-dependent adhesion proteins are up-regulated in *Capsaspora* aggregates (21, 47, 48). Therefore, the requirement of Ca^{2+} for *Capsaspora* aggregation may be to stabilize these adhesion molecules. In fact, we observed several cell–cell contacts

Downloaded from https://www.pnas.org by 84.18.99.124 on August 3, 2023 from IP address 84.18.99.124.

between filopodia of neighboring cells within aggregates, which may be the loci of these calcium-dependent cell–cell adhesion complexes. The exact mechanism of calcium-dependent aggregation is a topic of further research, but its general requirement is a similarity of aggregation induction in *Capsaspora* and sponges, as well as other animals and unicellular species.

The second chemical factor necessary to induce *Capsaspora* aggregation is a LDL, particularly the lipids present in LDLs. This inducer has similarities and differences with the aggregation inducers of other organisms—notably in their chemical composition, their source (environmental vs. organism-produced), and their general mechanism of action (signal vs. adhesive). Regarding the *composition* of the inducer itself, we are not aware of any organisms whose aggregation is induced by whole LDLs. LDLs are a similar size to sponge AFs, which are large soluble proteoglycans (37, 53, 66). This size affords the potential for multivalent interactions with the surfaces of one or more cells. In addition, the fact that lipids present in LDLs are the *Capsaspora* aggregation inducers also demonstrates some similarity with lipid kairomones that induce aggregation in some algae (50). In contrast, the inducer of choanoflagellate mating aggregation is a large protein enzyme (49), and *D. discoideum* and yeast aggregation are regulated by small molecules and peptides (51, 52). Regarding the *source* of the inducer, we have seen no evidence that *Capsaspora* secretes its aggregation inducer. Instead, it is likely an environmental cue, as are the inducers of aggregation in the choanoflagellate *Salpingoeca rosetta* and some algae (49, 50). Likewise, the *absence* of environmental nutrients plays a role in triggering aggregation in yeast and *D. discoideum*. In contrast, sponge AFs, as well as yeast pheromones and *D. discoideum* cAMP, are signals produced by the organism, itself. Finally, in terms of *mechanism*, it appears that only viable *Capsaspora* cells are capable of aggregating in response to lipoproteins and calcium ions. This finding suggests that these cues trigger an active cellular response, like cues do in yeast, *D. discoideum*, and algae—unlike sponge AFs, which act as adhesives to link even formalin-fixed cells. Therefore, although chemically regulated aggregation occurs in some animals, unicellular holozoans, and other unicellular eukaryotes, there is a wide range of inducers, sources, and mechanisms responsible.

The ecological and evolutionary relevance of lipoprotein-induced aggregation in *Capsaspora* is under additional investigation. *Capsaspora* has, so far, only been found inside snails (22, 64, 71), which do not possess classical LDLs or other types of vertebrate lipoproteins (63, 72). Therefore, it is possible that the LDL-mediated aggregation response is not relevant in *Capsaspora*'s natural environment. However, we found that reconstituted particles of sphingomyelin, phosphatidylcholine, cholesterol, triglyceride, and cholesteryl ester induced aggregation in *Capsaspora*. These lipids are common in animals, including *Biomphalaria* snails (73, 74). Therefore, it is plausible that *Capsaspora* aggregation is an evolved response to chemical cues from the snail host environment. Alternatively, *Capsaspora* may also live outside snail hosts where extracellular vesicles or other lipid/protein complexes from neighboring microbes may induce an aggregative behavior. In this case, the lipoprotein response could be ancient, even predating animals, as lipid signals are also known to trigger multicellular responses in other unicellular species (7, 50, 75). Indeed, phosphatidylcholines and sterols are commonly produced by microbial eukaryotes (76, 77), and some bacteria produce phosphatidylcholines and triglycerides as well (78, 79). Additionally, aggregation may be induced by other lipids that are not prevalent in LDLs but are ubiquitous in bacterial membranes (e.g., phosphatidylglycerols, phosphatidylethanolamines, and cardiolipins). Therefore, in ongoing work, we are comprehensively investigating which lipid classes induce aggregation and whether these components are also present in snail hosts or released by environmental microbes.

Taken together, the prevalence of chemically regulated aggregation, particularly in unicellular holozoans and some early branching animals, suggests that it is a broadly beneficial phenotype and therefore plausibly existed in the recent unicellular ancestors of animals. A remaining question is which mechanisms likely underpinned these phenotypes in their common unicellular ancestors—and if they continued to play important functions in the first animals. A route to address these questions is to characterize the genetic basis by which aggregation is regulated in *Capsaspora* and other unicellular holozoans and compare these to pathways employed in extant animals. If homologous genes are employed, then those steps could imply ancient conserved mechanisms of a regulated aggregation pathway. Importantly, our work identifying the inducers of aggregation will enable these essential investigations of the signaling pathways that initiate the *Capsaspora* aggregation process.

Conclusion

We discovered that the aggregative behavior of *Capsaspora* is a reversible process induced by a combination of calcium ions and lipids present in lipoproteins. Therefore, extant animals, other unicellular species, and this close unicellular relative to animals utilize chemical cues to regulate reversible aggregation. Similar to sponges, other animal species, and more distantly related unicellular organisms (e.g., yeasts and *D. discoideum*), *Capsaspora* requires calcium ions for aggregation. Although lipoproteins seem to be *Capsaspora*-specific cues, they resemble sponge AFs in their size and potential for multivalent interactions. Further characterization of the aggregation induction pathway in *Capsaspora* is warranted to determine the degree of conservation with extant animals. The results will help determine the likelihood that a regulated aggregation mechanism was a trait of the first animals. Furthermore, our findings combine with other recent studies to reveal a trend that unicellular holozoans utilize chemical triggers to regulate diverse multicellular phenotypes (49, 75). Although more taxa must be examined, these observations hint that soluble chemical cues were important in regulating reversible multicellularity in the close ancestors of animals.

Materials and Methods

See *SI Appendix* for full detailed *Materials and Methods*. Below is a summary.

Cell Strain and Growth Conditions. *Capsaspora owczarzaki* cell cultures (strain American Type Culture Collection (ATCC)® 30864) were grown axenically in 25-cm^2 culture flasks with 5 mL ATCC media 1,034 (modified PYNFH medium) containing 10% (v/v) heat-inactivated FBS, hereafter *growth media*, in a 23 °C incubator. Adherent stage cells (filopodiated amoebae) at the exponential growth phase were obtained by passaging ~100 to 150 µL adherent cells at ~90% confluence in 5 mL growth media and grown for 24 to 48 h at 23 °C.

General Aggregation Assay Methods. All aggregation assays were performed at room temperature. BF imaging was performed using the following instruments: Zeiss Axio Observer Z.1 epifluorescence inverted microscope equipped with LED illumination and an Axiocam 503 mono camera, Eclipse TS100 Nikon epifluorescence inverted microscope equipped with an Intensilight C-HGFI Illuminator and a DS-Fi2 Camera Head, A1 Nikon inverted microscope, and Leica DMi1 inverted microscope. Depending on well size and microscope used, each well was imaged at up to 36 distinct locations using 5× or 10× magnification. Average aggregate areas were measured by batch processing with a macro script in Fiji imaging software version 2.1.0/1.53c (80).

Downloaded from https://www.pnas.org by 84.18.99.124 on August 3, 2023 from IP address 84.18.99.124.

Aggregation assay using orbital agitation. Cells were washed and resuspended in growth media *without FBS* (8.33×10^6 cells/mL), seeded into a 12-well plate (7.5×10^5 cells per well), and starved at least 14 h. Putative aggregation inducers were added, and the plate was agitated at 50 rpm (Celltron Bench-Top Shaker, INFORS-HT). Typically aggregates were assessed by microscopy after 12 to 24 h. In some of the early experiments, adherent-stage cells were directly seeded in a 12-well plate (7.5×10^5 cells in 1 mL growth media) and incubated overnight (instead of starving 14 h in FBS-free media).

Aggregation assay without agitation. Cells were washed and resuspended in FBS-free media and allowed to starve overnight. After starvation, 8×10^5 cells were seeded in 160 µL FBS-free media per well in a 96-well ultralow attachment microplate (#CLS3474, Corning) and allowed to settle for 2 h. Putative aggregation inducers were added. Typically, aggregates were assessed by microscopy after 90 min.

FBS Contains Chemical Factor(s) Necessary for Aggregation in *Capsaspora*.

Media lacking component experiment (related to Fig. 2 A and B and SI Appendix, Fig. S1A). The standard aggregation assay with orbital agitation was used to assess activity of peptone-free media, yeast extract-free media, FBS-free media, 1× phosphate buffered saline (PBS), or full growth media.

Chemical Induction Is Sufficient for Aggregation Even in the Absence of Physical Agitation.

Aggregation dynamics over time in the absence of orbital agitation (related to Fig. 2C, SI Appendix, Fig. S1C, and Movies S1 and S2). The standard aggregation assay without orbital agitation was used to assess activity of 10% (v/v) and 30% (v/v) of FBS. The corresponding volume of 1× PBS was used as a negative control.

FBS dose–response experiment in orbital agitation (related to Fig. 2D and SI Appendix, Fig. S1B). The standard aggregation assay with orbital agitation was used to assess activity of 0 to 30% (v/v) of FBS.

FBS dose–response experiment in the absence of orbital agitation (related to Fig. 2 D–F, SI Appendix, Figs. S1D and S3, and Movies S3 and S4). The standard aggregation assay without orbital agitation was used to assess activity of 0 to 30% (v/v) of FBS (Fig. 2*D*). To monitor the dynamics of aggregation over time, either 0%, 0.5%, 1.5%, 5%, or 10% (v/v) of FBS was added in each well and imaged every 10 min for 42 h (Fig. 2 *E* and *F*, *SI Appendix*, Fig. S3, and Movies S3 and S4).

Chemical Induction of Aggregation is Reversible.

Reaggregation experiment in orbital agitation (related to SI Appendix, Figs. S1B and S4). Aggregation was induced using the standard aggregation assay in agitation conditions. After ~80 h, the cells had completely disaggregated, and reaggregation was induced by readding 10% (v/v) FBS per well. Sample supernatants from all time points (0 to 80 h) were collected to be further analyzed by western blot (related to Fig. 5*A* and *SI Appendix*, Fig. S12, see below).

Reaggregation experiment in the absence of orbital agitation (related to Fig. 2G, SI Appendix, Fig. S1C, and Movie S5). Aggregates were induced following the standard aggregation assay without orbital agitation. Cells were imaged every 3 min for 26 h, and after 9 min of imaging, aggregation was induced by the addition of 10% (v/v) of FBS. Once all cells had disaggregated (~19 h), an additional 30% (v/v) FBS or 30% (v/v) of 1× PBS (negative control) was readded to induce reaggregation.

Two Soluble FBS Components (One Small and One Large) Are Required for Aggregation.

Effect of FBS fractions on aggregation (related to Fig. 2H and SI Appendix, Fig. S1B). FBS was separated into >30-kDa and <30-kDa fractions with a 30-kDa MW cutoff filter. The <30-kDa flow-through was retained for testing, and the >30-kDa material was washed three times with PBS to minimize residual <30-kDa FBS material. Each fraction, as well as the combination of both, was assessed for activity using the standard aggregation assay with orbital agitation.

Effect of FBS fractions on reaggregation (related to Fig. 2I and SI Appendix, Fig. S1B). Aggregates were formed under the standard aggregation assay with orbital agitation. After ~72 h, the cells had completely disaggregated. At this point, 10% (v/v) of inducers (see above) were added, and cells were agitated another 1 to 2 h and assessed for reaggregation.

The Small Active Serum Component Is Calcium Ions.

Determination of active <3-kDa FBS fraction (related to SI Appendix, Fig. S5). FBS (15 mL) was passed through a 3-kDa MW cutoff filter, and the resulting ~15 mL that passed through the filter (corresponding to <3-kDa FBS material) was frozen and lyophilized to yield a powder. The resulting powder was dissolved in chloroform. The insoluble residue was dissolved in methanol. This process was repeated serially by dissolving insoluble residues with 80% methanol in water, 20% methanol in water, and finally 100% water. All dried supernatants (or the final remaining insoluble residue after water solubilization) were dissolved or resuspended in appropriate solvent, and activity of each combined with >30-kDa FBS was assessed using the agitation aggregation assay.

Calcium Ion quantification in FBS. Calcium ion content in FBS was quantified via a colorimetric assay (#MAK022, Sigma-Aldrich) following manufacturer's instructions. Results are represented as mean ± SD in three replicates.

Calcium rescue experiment (related to Fig. 3A and SI Appendix, Fig. S1D). The >30-kDa FBS fraction was washed three times with 1× PBS containing 0.5 M EGTA adjusted to pH 7 and then washed again 3 times more with 1× PBS to remove excess EGTA. A 5% (v/v) of washed >30-kDa FBS fraction was premixed with a 1:3 serial dilution of $CaCl_2$ diluted in 1× PBS (concentration range from 0.5 to 0 mM) and later added to each well. Aggregation was assessed under nonagitation conditions.

EGTA inhibition experiment (related to Fig. 3B and SI Appendix, Fig. S1D). FBS was mixed with a 1:3 serial dilution of EGTA (concentration range from 5 mM to 0 mM) diluted in 1× PBS and adjusted to pH 7 and later added to each well, reaching a final FBS concentration of 5% (v/v). Aggregation was assessed under nonagitation conditions.

Divalent cations dose–response experiments (related to Fig. 3C and SI Appendix, Fig. S1D). A 1:2 serial dilution (concentration range from 1 mM to 0 mM) of $CaCl_2$, $MgCl_2$, $MnCl_2$, $SrCl_2$, and $ZnCl_2$ was added to each well together with 5% (v/v) of >30-kDa FBS fraction, previously washed three times in 0.5 M EGTA diluted in 1× PBS and three more times with 1× PBS. Aggregation was assessed under nonagitation conditions.

The Combination of LDLs and Calcium Ions Is Sufficient to Induce Aggregation.

Protease treatment of >30-kDa FBS fraction (related to Fig. 4A). Protease treatment of >30-kDa FBS fraction was performed by treating 200 µL of large fraction (previously washed three times with 1× PBS) with 10 µL of 20 mg/mL Proteinase-K at 37 °C for 1 h, with periodic agitation. The proteinase was inactivated with 1 mM PMSF, and the sample was washed with a 30-kDa cutoff filter and resuspended to 200 µL (same volume as original sample). The aggregation activity of the protease-treated fraction was assessed with the agitation aggregation assay in combination with 0.2 mM $CaCl_2$.

Separation of >30-kDa FBS components by ammonium sulfate solubility (related to SI Appendix, Fig. S6). Whole FBS was washed and resuspended in 100 mM Tris-HCl, pH 8.0, 30-kDa MW cutoff filters. Proteins were fractionally precipitated from this sample by serial addition of ammonium sulfate at the following total concentrations: 20%, 30%, 40%, 50%, 55%, 60%, 65%, 70%, and 80%. Activity of each fraction was assessed with the aggregation assay in agitation conditions in combination with 0.2 mM $CaCl_2$.

Separation of active ammonium sulfate precipitate fraction by anion exchange chromatography (related to SI Appendix, Fig. S7). From the material that precipitated at 65% ammonium sulfate, a HiPrep Q XL 16/10 anion exchanger column was used at a 5 mL/min flow rate to separate this protein mixture using 20 mM ethanolamide/acetic acid buffer pH 9.2 with a gradient from 0 M NaCl (solvent A) to 1 M NaCl (solvent B). The gradient follows: 0 to 3 min (0% B), 3 to 38 min (linear gradient to 60% B), 38 to 40 min (linear gradient to 100% B), 40 to 45 min (hold 100% B). Activity of each fraction was assessed with the aggregation assay in agitation conditions in combination with 0.2 mM $CaCl_2$.

Separation of active anion exchange fractions by size exclusion chromatography (related to SI Appendix, Fig. S8). Active fractions from above were further separated through a Superdex 200 Increase 10/300 GL column with a 0.75 mL/min flow rate in 1× PBS pH 6.5. Activity of each fraction was assessed with the aggregation assay in agitation conditions in combination with 0.2 mM $CaCl_2$.

Determination of protein content of active size exclusion fractions via mass spectrometry of tryptic peptides (related to SI Appendix, Fig. S9 A and B and Dataset S1). The most active fractions from the size exclusion column were analyzed by SDS-PAGE and Coomassie staining. All visible unique bands (seven total) were excised and subjected to in-gel trypsin digestion and LC-MS/MS analysis by the Taplin Mass Spectrometry Facility at the Harvard Medical School. The major protein in all seven bands was Apolipoprotein B100 (ApoB100) (Dataset S1).

Downloaded from https://www.pnas.org by 84.18.99.124 on August 3, 2023 from IP address 84.18.99.124.

ApoB100 effect on Capsaspora aggregation (related to Fig. 4B and SI Appendix, Figs. S1A and S9C). The standard aggregation assay with orbital agitation was used to assess activity of several concentrations of commercial Apolipoprotein B100 (#A5353-0.5MG, Sigma-Aldrich) in combination with 0.3 mM $CaCl_2$.

Commercial LDL dose–response curve (related to Fig. 4C and SI Appendix, Fig. S1D). Commercial LDLs (#L7914, Sigma-Aldrich) were prewashed from their storage buffer with 30-kDa MW cutoff filters and resuspended in 1× PBS buffer. Their concentration was quantified by UV absorbance, assuming 25% protein content (65, 79). A range of concentrations (0 to 400 μg/mL) of LDL was assessed for activity in combination with 0.2 mM $CaCl_2$ using the nonagitation aggregation assay.

Whole FBS vs. LDL-deficient FBS dose–response curves (related to Fig. 4D and SI Appendix, Figs. S1D and S10D). The standard nonagitation aggregation assay was used to assess activity of 0 to 30% (v/v) of FBS (#MT35011CV, Corning) or lipoprotein-deficient FBS (#S5394, Sigma-Aldrich).

Western blots of FBS and LDL-deficient FBS (related to SI Appendix, Fig. S10 A and B). Equivalent volumes of FBS and LDL-deficient FBS were serially diluted with Laemmli loading buffer containing 5% (v/v) of 2-mercaptoethanol. After boiling, the samples were separated by SDS-PAGE and transferred to nitrocellulose membranes. Membranes were blocked with 5% (w/v) skimmed milk in 1× PBS with 0.1% (v/v) Tween-20. Proteins were probed with 1:2000 chicken anti-LDL primary antibody (#GW20089F, Sigma-Aldrich) and detected with 1:2000 HRP-conjugated goat anti-chicken secondary antibody (#A16054, Invitrogen). Samples were finally developed in a 1:1 mix of peroxide solution and luminol from the SuperSignal® West Pico Chemiluminescent Substrate (#34078, Thermo Fisher Scientific) and visualized in a ChemiDoc™ Touch Gel Imaging System Transilluminator (#1708370, Bio-Rad). Bands were quantified using Fiji imaging software version 2.1.0/1.53c (80).

Lipids Are the Active Components of LDLs.

Dose response of protein-free LDL-like particles (pfLDLs) (related to Fig. 4E and SI Appendix, Fig. S11 and Table S1). Protein-free LDL-like particles (pfLDLs) were prepared according to Vauhkonen *et al.*, (65) using the lipids POPC, 16:0 SM, cholesterol, triolein, and cholesteryl oleate in a 35:12:40:21:100 mol/mol lipid mixture. The pfLDLs were resuspended in 1× PBS buffer. The standard nonagitation aggregation assay was used to assess their activity at 0 to 153 μg/mL in combination with 0.2 mM $CaCl_2$. The size distribution of particles was confirmed using a DLS Zetasizer Nano and JEOL JEM 1010 TEM, and the composition of particles was verified by LCMS using Waters Synapt G2S QTOF.

Dynamic Lipoprotein Concentration Regulates the Aggregative State of *Capsaspora*.

LDL depletion experiment (related to Fig. 5A and SI Appendix, Figs. S4 A and B and S12). To assess LDL depletion over time, aggregates were induced with 10% (v/v) FBS using orbital agitation and monitored during 80 h (see *Reaggregation experiment in orbital agitation, related to SI Appendix*, Figs. S1*B* and S3 *assay).* Cell supernatant was collected at each time point, diluted with loading buffer, and subjected to SDS-PAGE and western blotting as above.

Immunofluorescence microscopy (related to Fig. 5B). Aggregates were fixed in a 4% formaldehyde concentration, washed with PBS, blocked with blocking solution (1% BSA and 0.1% Triton X-100 in 1× PBS), and stained with chicken anti-LDL primary antibody (#GW20089F, Sigma-Aldrich) and goat anti-chicken Alexa Fluor 488 secondary antibody (#H11039, Invitrogen). Cells were counterstained with Alexa Fluor™ 350 Phalloidin (#A22281, Thermo Fisher Scientific) and DRAQ5 (#62251, Thermo Fisher Scientific) before mounting onto poly-L-lysine-coated coverslips with ProLong Gold Antifade Reagent (#P36930, Thermo Fisher Scientific) and observing at 40× magnification on a Leica TCS SP5 II inverted confocal microscope.

Only Viable *Capsaspora* Cells Aggregate.

Aggregation induction in formalinized cells (related to Fig. 5C and SI Appendix, Fig. S1B). Adherent-stage cells were washed and resuspended in 500 μL 1× PBS containing 0.3 mM $CaCl_2$ and 0.3 mM $MgCl_2$. Next, an additional 500 μL containing 0 to 32% of increasing concentrations of formaldehyde diluted in the previous buffer solution was added for each condition. Samples were homogenized by gently pipetting and fixed for 10 min on a rotating shaker. After fixation, cells were washed with 1 mL of the previous buffer solution, resuspended in growth media (containing 10% FBS), and assessed following the aggregation assay in agitation conditions.

Data, Materials, and Software Availability. All study data are included in the article and/or *SI Appendix*.

ACKNOWLEDGMENTS. We thank the Light Microscopy Center at the Indiana University for support in image acquisition and analysis (funding provided by the NIH grant NIH1S10OD024988-01) and the Advanced Light Microscopy Unit of the Center for Genomic Regulation for support on image acquisition. We also thank the Indiana University Nanoscale Characterization Facility, Electron Microscopy Center, and Laboratory for Biological Mass Spectrometry for use of their instruments. We want to special thank Claudio Scazzocchio for fruitful discussions and Sebastián R. Najle for feedback and support in early work on *Capsaspora* aggregation. We acknowledge Omaya Dudin for feedback and support in image acquisition and analysis, Michelle M. Leger for feedback on the manuscript, and Koryu Kin for support in immunocytochemistry experiments, image acquisition and analysis, and stimulating discussions. We also thank many people from the lab for insights and support that helped advance this project. This work was supported by a NIH grant (R35GM138376) to J.P.G. and grants BFU2017-90114-P from Ministerio de Economía y Competitividad, Agencia Estatal de Investigación (AEI), and Fondo Europeo de Desarrollo Regional and PID2020-120609GB-I00 by Ministerio de Ciencia e Innovación/AEI/10.13039/501100011033 and "European Regional Development Fund: A way of making Europe" to I.R.-T. N.R.-R. was supported by a "Formación del Profesorado Universitario (FPU13/01840)" predoctoral fellowship from Ministerio de Educación, Cultura y Deporte and R.Q.K. was supported by a NIH training grant (T32GM131994).

1. R. K. Grosberg, R. R. Strathmann, The evolution of multicellularity: A minor major transition? *Annu. Rev. Ecol. Evol. Syst.* **38**, 621–654 (2007).
2. S. M. Adl *et al.*, Revisions to the classification, nomenclature, and diversity of eukaryotes. *J. Eukaryotic Microbiol.* **66**, 4–119 (2019).
3. M. Brown, J. Silberman, "The non-dictyostelid sorocarpic amoebae" in *Dictyostelids: Evolution Genomics Cell Biology*, M. Romeralo, S. Baldauf, R. Escalante, Eds. (Springer, 2013), pp. 219–242.
4. F. Burki, A. J. Roger, M. W. Brown, A. G. B. Simpson, The new tree of eukaryotes. *Trends Ecol. Evol.* **35**, 43–55 (2020).
5. A. Sebé-Pedrós, B. M. Degnan, I. Ruiz-Trillo, The origin of metazoa: A unicellular perspective. *Nat. Rev. Genet* **18**, 498–512 (2017).
6. M. La Fortezza, K. Schaal, G. J. Velicer, Why aggregate? On the evolution of aggregative multicellularity (2021). https:/doi.org/10.20944/preprints202105.0451.v1 (Accessed 14 October 2021).
7. Q. Du, Y. Kawabe, C. Schilde, Z. Chen, P. Schaap, The evolution of aggregative multicellularity and cell-cell communication in the dictyostelia. *J. Mol. Biol.* **427**, 3722–3733 (2015).
8. P. Schaap, Evolutionary crossroads in developmental biology: Dictyostelium discoideum. *Development* **138**, 387–396 (2011).
9. M. Brown, J. D. Silberman, F. W. Spiegel, Slime molds among the tubulinea (Amoebozoa): Molecular systematics and taxonomy of copromyxa. *Protist* **162**, 277–287 (2011).
10. M. Brown, M. Kolisko, J. D. Silberman, A. J. Roger, Aggregative multicellularity evolved independently in the eukaryotic supergroup rhizaria. *Curr. Biol.* **22**, 1123–1127 (2012).
11. M. W. Brown, J. D. Silberman, F. W. Spiegel, A contemporary evaluation of the acrasids (Acrasidae, Heterolobosea, Excavata). *Eur. J. Protistol.* **48**, 103–123 (2012).
12. M. J. Dykstra, L. S. Olive, Sorodiplophrys: An unusual sorocarp-producing protist. *Mycologia* **67**, 873–879 (1975).
13. L. S. Olive, R. L. Blanton, Aerial sorocarp development by the aggregative ciliate. *Sorogena Stoianovitchae*. *J. Protozool.* **27**, 293–299 (1980).
14. S. Sathe, P. M. Durand, Cellular aggregation in chlamydomonas (Chlorophyceae) is chimaeric and depends on traits like cell size and motility. *Eur. J. Phycol.* **51**, 129–138 (2016).
15. A. K. Tice *et al.*, Sorodiplophrys stercorea: Another novel lineage of sorocarpic multicellularity. *J. Eukaryot Microbiol.* **63**, 623–628 (2016).
16. M. W. Brown, F. W. Spiegel, J. D. Silberman, Phylogeny of the "Forgotten" cellular slime mold, fonticula alba, reveals a key evolutionary branch within opisthokonta. *Mol. Biol. Evol.* **26**, 2699–2709 (2009).
17. X. Grau-Bové *et al.*, Dynamics of genomic innovation in the unicellular ancestry of animals. *eLife* **6**, e26036 (2017).
18. E. Hehenberger *et al.*, Novel predators reshape holozoan phylogeny and reveal the presence of a two-component signaling system in the ancestor of animals. *Curr. Biol.* **27**, 2043–2050.e6 (2017).
19. G. Torruella *et al.*, Phylogenomics reveals convergent evolution of lifestyles in close relatives of animals and fungi. *Curr. Biol.* **25**, 2404–2410 (2015).
20. E. Ocaña-Pallarès *et al.*, Divergent genomic trajectories predate the origin of animals and fungi. *Nature* **609**, 747–753 (2022).
21. A. Sebé-Pedrós *et al.*, Regulated aggregative multicellularity in a close unicellular relative of metazoa. *eLife* **2**, e01287 (2013).
22. H. H. Stibbs, A. Owczarzak, C. J. Bayne, P. DeWan, Schistosome sporocyst-killing amoebae isolated from biomphalaria glabrata. *J. Invertebr. Pathol.* **33**, 159–170 (1979).

Downloaded from https://www.pnas.org by 84.18.99.124 on August 3, 2023 from IP address 84.18.99.124.

23. A. Ereskovsky, E. Renard, C. Borchiellini, Cellular and molecular processes leading to embryo formation in sponges: Evidences for high conservation of processes throughout animal evolution. *Dev. Genes Evol.* **223**, 5–22 (2013).
24. A. Kirillova *et al.*, Germ-layer commitment and axis formation in sea anemone embryonic cell aggregates. *Proc. Natl. Acad. Sci. U.S.A.* **115**, 1813–1818 (2018).
25. R. M. Savage, M. V. Danilchik, Dynamics of germ plasm localization and its inhibition by ultraviolet irradiation in early cleavage xenopus embryos. *Dev. Biol.* **157**, 371–382 (1993).
26. M. L. Costa, I. de Andrade Rosa, L. Andrade, C. Mermelstein, C. C. Coutinho, Distinct interactions between epithelial and mesenchymal cells control cell morphology and collective migration during sponge epithelial to mesenchymal transition. *J. Morphol.* **281**, 183–195 (2019).
27. P. Powan, P. Chanvorachote, Nitric oxide mediates cell aggregation and mesenchymal to epithelial transition in anoikis-resistant lung cancer cells. *Mol. Cell Biochem.* **393**, 237–245 (2014).
28. D. Eerkes-Medrano, C. J. Feehan, S. P. Leys, Sponge cell aggregation: Checkpoints in development indicate a high level of organismal complexity. *Invertebr. Biol.* **134**, 1–18 (2014).
29. A. Ereskovsky, I. E. Borisenko, F. V. Bolshakov, A. I. Lavrov, Whole-body regeneration in sponges: Diversity, fine mechanisms, and future prospects. *Genes (Basel)* **12**, 506 (2021).
30. C. Ferrario, M. Sugni, I. M. L. Somorjai, L. Ballarin, Beyond adult stem cells: Dedifferentiation as a unifying mechanism underlying regeneration in invertebrate deuterostomes. *Front. Cell Dev. Biol.* **8**, 587320 (2020).
31. J. Girstmair, R. Schnegg, M. J. Telford, B. Egger, Cellular dynamics during regeneration of the flatworm monocelis sp. (Proseriata, Platyhelminthes). *EvoDevo* **5**, 37 (2014).
32. A. Ruthmann, U. Terwelp, Disaggregation and reaggregation of cells of the primitive metazoon trichoplax adhaerens. *Differentiation* **13**, 185–198 (1979).
33. T. C. G. Bosch, Why polyps regenerate and we don't: Towards a cellular and molecular framework for Hydra regeneration. *Dev. Biol.* **303**, 421–433 (2007).
34. A. W. Seifert, K. Muneoka, The blastema and epimorphic regeneration in mammals. *Dev. Biol.* **433**, 190–199 (2018).
35. A. Soubigou, E. G. Ross, Y. Touhami, N. Chrismas, V. Modepalli, Regeneration in the sponge sycon ciliatum partly mimics postlarval development. *Development* **147**, dev193714 (2020).
36. J. K. Parrish, L. Edelstein-Keshet, Complexity, pattern, and evolutionary trade-offs in animal aggregation. *Science* **284**, 99–101 (1999).
37. P. Henkart, S. Humphreys, T. Humphreys, Characterization of sponge aggregation factor. A unique proteoglycan complex. *Biochemistry* **12**, 3045–3050 (1973).
38. J. E. Jumblatt, V. Schlup, M. M. Burger, Cell-cell recognition: Specific binding of microciona sponge aggregation factor to homotypic cells and the role of calcium ions. *Biochemistry* **19**, 1038–1042 (1980).
39. K. W. Jones, T. R. Elsdale, The culture of small aggregates of amphibian embryonic cells in vitro. *J. Embryol. Exp. Morphol.* **11**, 135–154 (1963).
40. M. Matsuda, Serum proteins enhance aggregate formation of dissociated fetal rat brain cells in an aggregating culture. *Vitro Cell Dev. Biol.* **24**, 1031–1036 (1988).
41. J. L. Miller, J. M. Kupinski, A. Castella, Z. M. Ruggeri, Von willebrand factor binds to platelets and induces aggregation in platelet-type but not type IIB von willebrand disease. *J. Clin. Invest.* **72**, 1532–1542 (1983).
42. W. E. Müller, A. Dorn, G. Uhlenbruck, The molecular mechanisms of the distinct calcium-dependent aggregation systems in marine sponges and corals. *Acta Histochem. Suppl.* **31**, 37–46 (1985).
43. N. Ros-Rocher, A. Pérez-Posada, M. M. Leger, I. Ruiz-Trillo, The origin of animals: An ancestral reconstruction of the unicellular-to-multicellular transition. *Open Biol.* **11**, 200359 (2021).
44. B. Goldstein, N. King, The future of cell biology: Emerging model organisms. *Trends Cell Biol.* **26**, 818–824 (2016).
45. T. Brunet, N. King, The origin of animal multicellularity and cell differentiation. *Dev. Cell* **43**, 124–140 (2017).
46. D. V. Tikhonenkov *et al.*, Insights into the origin of metazoan multicellularity from predatory unicellular relatives of animals. *BMC Biol.* **18**, 39 (2020).
47. A. Sebé-Pedrós *et al.*, High-throughput proteomics reveals the unicellular roots of animal phosphosignaling and cell differentiation. *Dev. Cell* **39**, 186–197 (2016).
48. A. Sebé-Pedrós *et al.*, The dynamic regulatory genome of capsaspora and the origin of animal multicellularity. *Cell* **165**, 1224–1237 (2016).
49. A. Woznica, J. P. Gerdt, R. E. Hulett, J. Clardy, N. King, Mating in the closest living relatives of animals is induced by a bacterial chondroitinase. *Cell* **170**, 1175–1183.e11 (2017).
50. K. Yasumoto *et al.*, Isolation of new aliphatic sulfates and sulfamate as the daphnia kairomones inducing morphological change of a phytoplankton scenedesmus gutwinskii. *Chem. Pharm. Bull. (Tokyo)* **56**, 133–136 (2008).
51. P. Schaap, Evolution of developmental cyclic adenosine monophosphate signaling in the dictyostelia from an amoebozoan stress response. *Dev. Growth Differ.* **53**, 452–462 (2011).
52. J. A. Vallejo, A. Sánchez-Pérez, J. P. Martínez, T. G. Villa, Cell aggregations in yeasts and their applications. *Appl. Microbiol. Biotechnol.* **97**, 2305–2318 (2013).
53. L. F. Grice *et al.*, Origin and evolution of the sponge aggregation factor gene family. *Mol. Biol. Evol.* **34**, 1083–1099 (2017).
54. A. I. Lavrov, I. A. Kosevich, Sponge cell reaggregation: Mechanisms and dynamics of the process. *Russ. J. Dev. Biol.* **45**, 205–223 (2014).
55. A. I. Lavrov, I. A. Kosevich, Sponge cell reaggregation: Cellular structure and morphogenetic potencies of multicellular aggregates. *J. Exp. Zool. A Ecol. Genet. Physiol.* **325**, 158–177 (2016).
56. T. Lindl, *Zell- und Gewebekultur* (Spektrum Akademischer Verlag, ed. 5, 2002).
57. I. S. Gul, P. Hulpiau, Y. Saeys, F. van Roy, Evolution and diversity of cadherins and catenins. *Exp. Cell Res.* **358**, 3–9 (2017).
58. Y. Poloz, D. H. O'Day, Colchicine affects cell motility, pattern formation and stalk cell differentiation in dictyostelium by altering calcium signaling. *Differentiation* **83**, 185–199 (2012).
59. D. Vicogne *et al.*, Fetal bovine serum impacts the observed N-glycosylation defects in TMEM165 KO HEK cells. *J. Inherit. Metab. Dis.* **43**, 357–366 (2020).
60. K. R. Feingold, Introduction to lipids and lipoproteins (March 9, 2022), MDText.com Inc, 2000. Available at https://www.ncbi.nlm.nih.gov/books/NBK305896/.
61. J. P. Segrest, M. K. Jones, H. D. Loof, N. Dashti, Structure of apolipoprotein B-100 in low density lipoproteins. *J. Lipid Res.* **42**, 1346–1367 (2001).
62. S. Morita, Y. Deharu, E. Takata, M. Nakano, T. Handa, Cytotoxicity of lipid-free apolipoprotein B. *Biochim. Biophys. Acta* **1778**, 2594–2603 (2008).
63. J.-Q. Liu *et al.*, Gain and loss events in the evolution of the apolipoprotein family in vertebrata. *BMC Evol. Biol.* **19**, 209 (2019).
64. A. Owczarzak, H. H. Stibbs, C. J. Bayne, The destruction of schistosoma mansoni mother sporocysts in vitro by amoebae isolated from biomphalaria glabrata: An ultrastructural study. *J. Invertebr. Pathol.* **35**, 26–33 (1980).
65. M. Vauhkonen, P. Somerharju, The surface lipid layer of human low density lipoprotein probed by dipyrenyl phospholipids. *Chem. Phys. Lipids* **52**, 207–216 (1990).
66. A. Leith, Role of aggregation factor and cell type in sponge cell adhesion. *Biol. Bull.* **156**, 212–223 (1979).
67. J. E. Phillips, M. Santos, M. Konchwala, C. Xing, D. Pan, Genome editing in the unicellular holozoan capsaspora owczarzaki suggests a premetazoan role for the hippo pathway in multicellular morphogenesis. *eLife* **11**, e77598 (2022).
68. D. E. Clapham, Calcium signaling. *Cell* **131**, 1047–1058 (2007).
69. R. Kemler, M. Ozawa, M. Ringwald, Calcium-dependent cell adhesion molecules. *Curr. Opin. Cell Biol.* **1**, 892–897 (1989).
70. D. Kirchhofer, J. Grzesiak, M. D. Pierschbacher, Calcium as a potential physiological regulator of integrin-mediated cell adhesion. *J. Biol. Chem.* **266**, 4471–4477 (1991).
71. L. A. Hertel, C. J. Bayne, E. S. Loker, The symbiont capsaspora owczarzaki, nov. gen. nov. sp., isolated from three strains of the pulmonate snail biomphalaria glabrata is related to members of the mesomycetozoea. *Int. J. Parasitol.* **32**, 1183–1191 (2002).
72. R. J. Pollero, M. R. González-Baró, C. Garín, Lipid transport in snails. Partial characterization of a high-density lipoprotein isolated from ampullaria canaliculata plasma. *Com. Biochem. Physiol. Part B: Com. Biochem.* **102**, 717–720 (1992).
73. P. H. Shetty, B. Fried, J. Sherma, Sterols in the plasma and digestive gland-gonad complex of biomphalaria glabrata snails, fed lettuce versus hen's egg yolk, as determined by GLC. *Comp. Biochem. Physiol. B* **96**, 791–794 (1990).
74. D. Allan, G. Payares, W. H. Evans, The phospholipid and fatty acid composition of schistosoma mansoni and of its purified tegumental membranes. *Mol. Biochem. Parasitol.* **23**, 123–128 (1987).
75. R. A. Alegado *et al.*, A bacterial sulfonolipid triggers multicellular development in the closest living relatives of animals. *eLife* **1**, e00013 (2012).
76. A. Lykidis, Comparative genomics and evolution of eukaryotic phospholipid biosynthesis. *Prog. Lipid. Res.* **46**, 171–199 (2007).
77. E. Desmond, S. Gribaldo, Phylogenomics of sterol synthesis: Insights into the origin, evolution, and diversity of a key eukaryotic feature. *Genome Biol. Evol.* **1**, 364–381 (2009).
78. F. Martínez-Morales, M. Schobert, I. M. López-Lara, O. Geiger, Pathways for phosphatidylcholine biosynthesis in bacteria. *Microbiology (Reading)* **149**, 3461–3471 (2003).
79. H. M. Alvarez, A. Steinbüchel, Triacylglycerols in prokaryotic microorganisms. *Appl. Microbiol. Biotechnol.* **60**, 367–376 (2002).
80. J. Schindelin *et al.*, Fiji: An open-source platform for biological-image analysis. *Nat. Methods* **9**, 676–682 (2012).

Downloaded from https://www.pnas.org by 84.18.99.124 on August 3, 2023 from IP address 84.18.99.124.